X-614-67-90

NASA TM X-55922

THE SOLAR CORONA ABOVE ACTIVE REGIONS: A COMPARISON OF EXTREME ULTRAVIOLET LINE EMISSION WITH RADIO EMISSION

BY

WERNER M. NEUPERT

MARCH 1967

NASA

GODDARD SPACE FLIGHT CENTER

GREENBELT, MARYLAND

THE SOLAR CORONA ABOVE ACTIVE REGIONS: A COMPARISON OF EXTREME ULTRAVIOLET LINE EMISSION WITH RADIO EMISSION

By

Werner M. Neupert
Goddard Space Flight Center
Greenbelt, Maryland

ABSTRACT

The observation of extreme ultraviolet (EUV) emission lines of Fe IX through Fe XVI made by OSO-1 are discussed and applied to a study of the solar corona above active regions. Ultraviolet and radio emission are determined for several levels of activity classified according to the type of sunspot group associated with the active region. Both radio emission and line radiation from Fe XVI, the highest stage of ionization of Fe observed, are observed to increase rapidly with the onset of activity and are most intense over an E spot group early in the lifetime of the active region. As activity diminishes, radiation from Fe XV and Fe XIV becomes relatively more prominent. The observations imply that the coronal temperature reaches a maximum during the period of highest activity, as indicated by sunspot group complexity and the occurrence of chromospheric flares. A maximum coronal temperature of 3.8 - 10^6 °K is estimated when taking into account the mechanism of dielectronic recombination. Concurrently, the coronal electron density increases by a factor of 10 - 12. Both electron temperature and density decrease as activity subsides. A value of 2.5 - 3.0 x 10^6 °K is obtained after flare activity has ceased and sunspots have disappeared.

I. INTRODUCTION

With the advent of rockets and satellites, it has become possible to make observations of permitted emission lines originating in the solar corona above active regions as these regions pass across the visible solar disk. The extreme ultraviolet (EUV) observations made by the first Orbiting Solar Observatory (OSO-1), launched on March 7, 1962, present the first and as yet only opportunity for such a study over an extended period of time. Contained in the scientific payload of this satellite was a spectrometer (Behring, Neupert and Nichols, 1962) for recording the solar spectrum in the wavelength range from λ150 to λ400. The coronal emission lines of many elements were recorded for a time interval greater than one year and during a wide range of solar activity (Behring, Neupert and Lindsay, 1963). The observed twenty-seven day variations in line intensities attributable to this activity have been discussed previously (Neupert, 1965).

Spectrograms in the same spectral range (Hinteregger, 1961; Tousey, 1965), taken during rocket flights and therefore made without the benefit of a long observing interval have already been used for analyses of the solar atmosphere. Pottasch (1963) has applied simultaneous EUV and radio measurements to the study the distribution of electron density as a function of temperature in the transition region and corona. Unfortunately, the observations he used (Detwiler, Garrett, Purcell, and Tousey, 1961, and Hinteregger, 1961) did not allow him to distinguish

between emission from active regions and emission from the undisturbed corona. Jordan (1966) and Pottasch (1966) have discussed the abundance of heavier elements as derived from the EUV data, finding that in the corona the abundance of iron, in particular, may be greater by a factor of 10 than its value in the photosphere. This conclusion has recently been questioned by Athay (1966). Dirin and Dietz (1963) have discussed in detail how EUV observations can be used in analysing the structure of the solar chromosphere while Widing (1966) has used more recent rocket observations (Austin, Purcell, Tousey and Widing, 1966) to discuss the soft x-ray spectrum of the sun with primary emphasis on the spectrum of the quiet corona.

EUV spectra of the entire sun have recently been supplemented by slitless spectra (Tousey, 1965) which demonstrate directly the tendency for emission lines from the most hightly ionized ions to be most intense over active regions. Because such studies have been made from rockets, no sequential study over the lifetime of any one region has been possible. The present paper attempts to describe in more detail the EUV and radio emissions of several specific active regions as they develope with time. Our ability to discuss this problem using the OSO-1 data is limited by the fact that these observations provided no spatial resolution. The analysis is made possible only by the circumstance that OSO-1 observed the sun during the declining portion of the last solar cycle when the appearances of relatively

few active centers were interspersed with periods of low solar activity. We will first determine the line emission in selected EUV lines and the simultaneous radio microwave emission from the corona over an active region at several characteristic stages of its development. We then will consider a model of the coronal region and use the collected data to obtain estimates of the electron temperature density and the abundance of iron for the regions which were observed.

II. EXTREME ULTRAVIOLET OBSERVATIONS BY OSO-1

Since many of the emission lines observed by OSO-1 in the extreme ultraviolet (Figure 1) still lack reliable identifications, or are blended with neighboring lines, we restrict ourselves to a series of intense, well-resolved lines now known to be emission lines of iron. Identification of these lines has proceeded rapidly in the past several years, with research groups at Culham Laboratory (Fawcett and Gabriel, 1965, Fawcett, Gabriel, and Saunders, 1966), Los Alamos Scientific Laboratories (Cowan and Peacock, 1965) Hebrew University (Alexander, Feldman, Fraenkel, and Hoory, 1965), the High Altitude Observatory (House, Deutschman and Sawyer, 1964), and the Naval Research Laboratory (Elton, Kolb, Austin, Tousey, and Widing, 1964) agreeing on the identification of an ever increasing number of solar lines which have been reproduced in plasma pinches and high energy sparks. In this paper we use the results obtained by these groups, and in addition, identifications originally

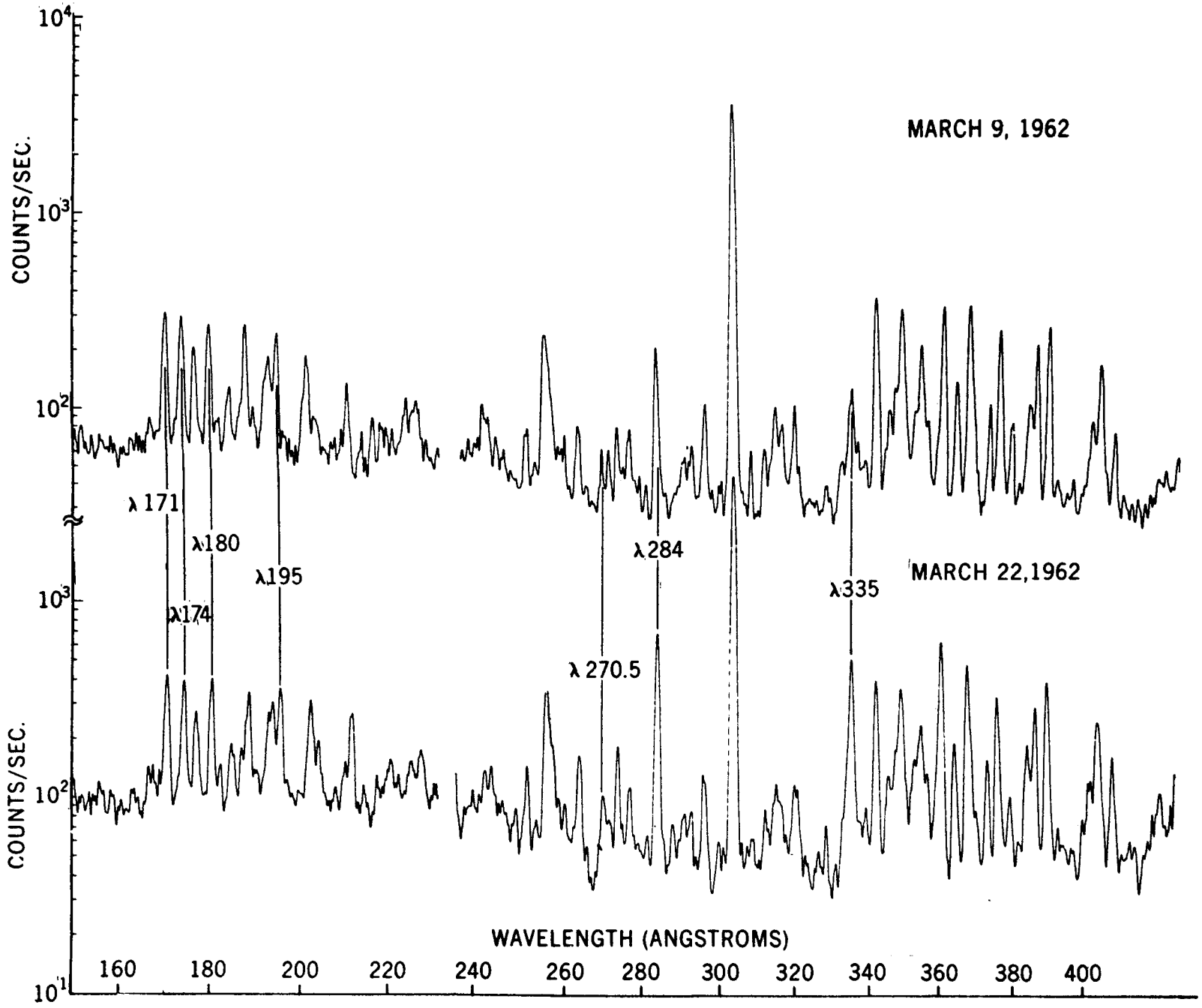
MARCH 9, 1962
MARCH 22,1962
COUNTS/SEC.
COUNTS/SEC.
λ 171
λ174
λ180
λ195
λ 270.5
λ284
λ335
WAVELENGTH (ANGSTROMS)
160
180
200
220
240
260
280
300
320
340
360
380
400

suggested for Fe XIV by Neupert and Smith (1964) on the basis of variations of line intensities with varying solar activity. Here we will present data for only one line in each stage of ionization, choosing those lines which are most reliably identified and have greatest statistical accuracy. These lines are given in Table I together with the electron temperature at which each ion has its maximum relative abundance (Burgess and Seaton, 1964). The estimated intensity of each line during an interval of very low solar activity, March 9-11, is also given.

The OSC-1 EUV spectrometer recorded radiation from the entire visible solar hemisphere at all times, so that the observed counting rate in any spectral line represents the combined emission from all active centers as well as any radiation emitted by the undisturbed solar atmosphere. We have been able to discriminate between these two components by comparing data taken when the sun was devoid of any active regions to data taken when one or more active regions were present on the visible solar disk. The first "quiet sun" period, on March 9-11, was characterized by a Zürich Relative Sunspot Number very close to zero and by the lowest CaII plage area observed during the two and one-half month interval of continuous observation. The hemisphere of the sun turned toward the earth at that time had produced no active centers during the preceding six months. Minimum counting rates were observed for nearly every EUV spectral line thus far examined and have been designated as "quiet sun" observations. All subsequent EUV data are normalized to these

TABLE I

ION	WAVELENGTH	TRANSITION	ΔJ	T_e for Maximum Abundance	Estimated Flux March 8-10, 1962
Fe IX	171.1A	$3p^6\ {}^1S - 3p^5\ 3d\ {}^1P^0$	0-1	$.95 \times 10^6$ °K	6.8×10^7 ph $cm^{-2}sec^{-1}$
Fe X	174.6	$3p^5\ {}^2P^0 - 3p^4({}^1D)\ 3d\ {}^2P$	1½-1½	1.15	6.2×10^7
Fe XI	180.5	$3p^4\ {}^3P - 3p^3({}^2P)\ 3d\ {}^3D^0$	2-3	1.45	6.0×10^7
Fe XII	188.4	Blend with Fe XI		1.75	4.9×10^7
Fe XIII	195.0	$3p^3\ {}^4S^0 - 3p^2({}^3P)\ 3d\ {}^4P$	1½-2½	2.00	4.6×10^7
Fe XIV	270.5	$3s^2\ 3p\ {}^2P^0 - 3s\ 3p^2\ {}^2P$	1½-½	2.30	1.3×10^7
Fe XV	284.1	$3s^2\ {}^1S - 3s\ 3p\ {}^1P$	0-1	2.75	7.4×10^7
Fe XVI	335.5	$3s\ {}^2S - 3p\ {}^2P^0$	½-1½	4.0	9.8×10^7

observations. We refer to any increases above a value of one as "relative enhancements" and assume that they are due to the presence of active regions on the solar disk.

The OSO-1 data available for analysis of the slowly varying component of solar emission are presented in Figure 2. On the left-hand side are shown the intensity variations of the iron lines, and on the right-hand side the radio measurements for the same interval of time as obtained from the I.A.U. Quarterly Bulletin on Solar Activity. Both sets of data exhibit gradual changes in the shapes of the curves as these progress from low to high stage of ionization and from low frequency to high frequency in the radio spectrum. The relationship between these data have been studied using a least squares fit of the radio fluxes to the EUV observations. Slightly smaller standard deviations of the residuals are obtained when a quadratic is used than when a linear relationship is assumed. Results for Fe XV and Fe XVI, shown in Figure 3, suggest that the variations of the highest stages of ionization of Fe which we have observed - Fe XVI and Fe XV - resemble most strongly the radio observations at frequencies around 2000 MHz. Emission lines from lower stages of ionization correlate less well with radio fluxes and show no distinct association with either the higher or the lower range of frequencies although it appears that some fluctuations occurring over a period of only a few days, for example, April 18 to April 24 can be traced through successively lower stages of

COMPARISON OF SOLAR EUV AND RADIO OBSERVATIONS
(MARCH - MAY 1962)

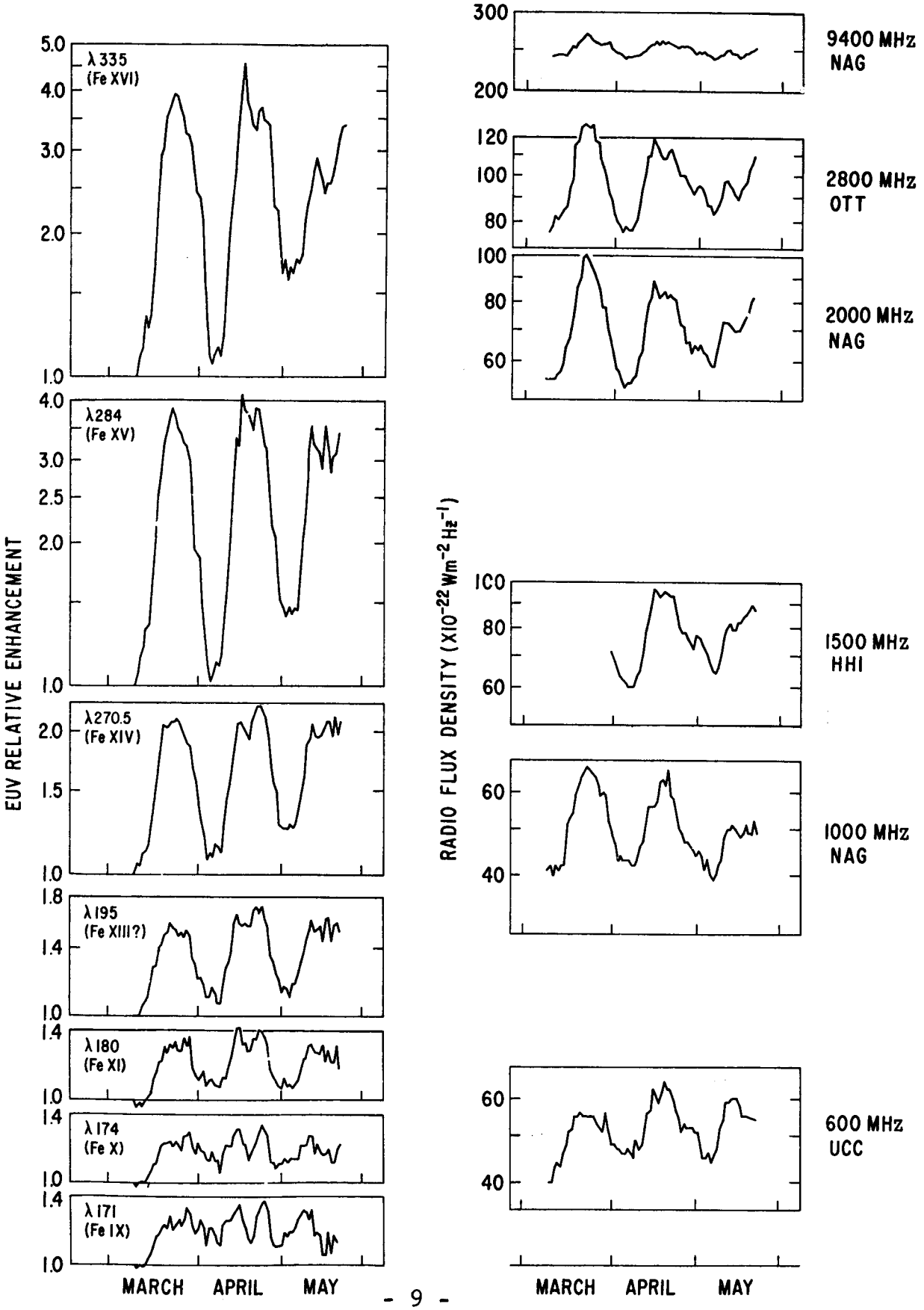

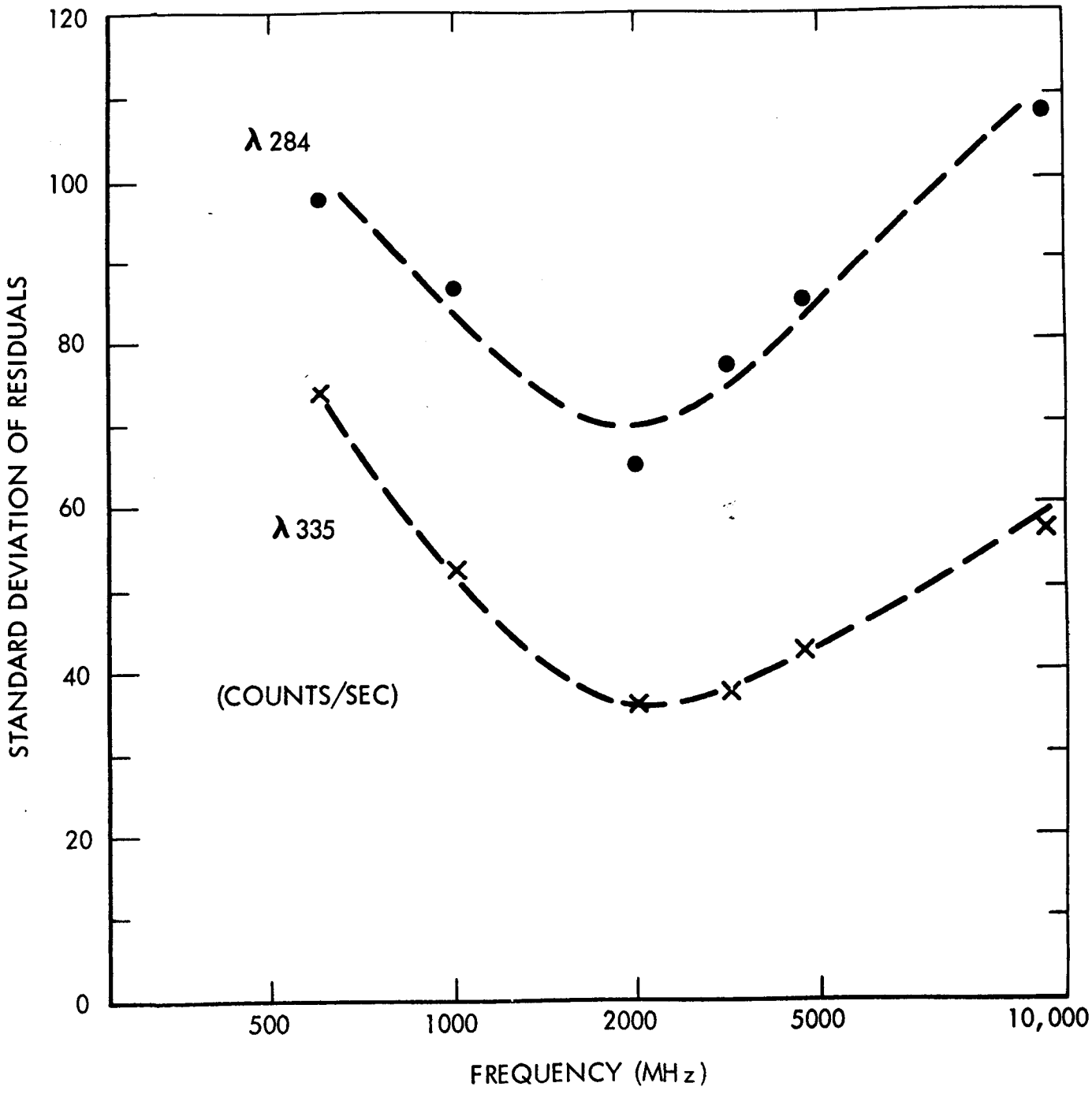
120
100
80
60
40
20
0
λ 284
λ 335
(COUNTS/SEC)
STANDARD DEVIATION OF RESIDUALS
500
1000
2000
5000
10,000
FREQUENCY (MHz)

ionization and also through the entire range of radio frequencies.

From these data it is possible to extract two sequences of observations, shown in Figures 4 and 5, which are particularly valuable in describing the changes in EUV and radio emission from the corona above active centers. In these figures the observed relative enhancement of one emission line for each ion is plotted against the temperature at which that ion has its maximum abundance relative to other stages of ionization of the same element. For the radio fluxes the observed excess over the flux observed on March 9-11 is plotted against the frequency at which the measurement is made. The sequence shown in Figure 4 began with the development of a small spot group, reported by the Fraunhofer Institut as belonging to Class B5 (bipolar group without penumbra in the Zürich classification) on April 6. Neither the EUV radiations of Fe XIV through Fe XVI nor the decimetric radio emission showed an increase over the fluxes observed on March 9-11, when no active centers were present on the visible solar disk. At its next meridian passage, on May 1, the spot group observed on April 6 had developed to C11 (bipolar group, like B, but at least one main spot with penumbra) and the Ca II plage associated with this center had increased to 5000 millionths of the solar hemisphere. The center had become a strong emitter of Fe XV and Fe XVI radiations as well as decimetric radio fluxes. Because of a spacecraft malfunction, no observations were made at the next central meridian passage of

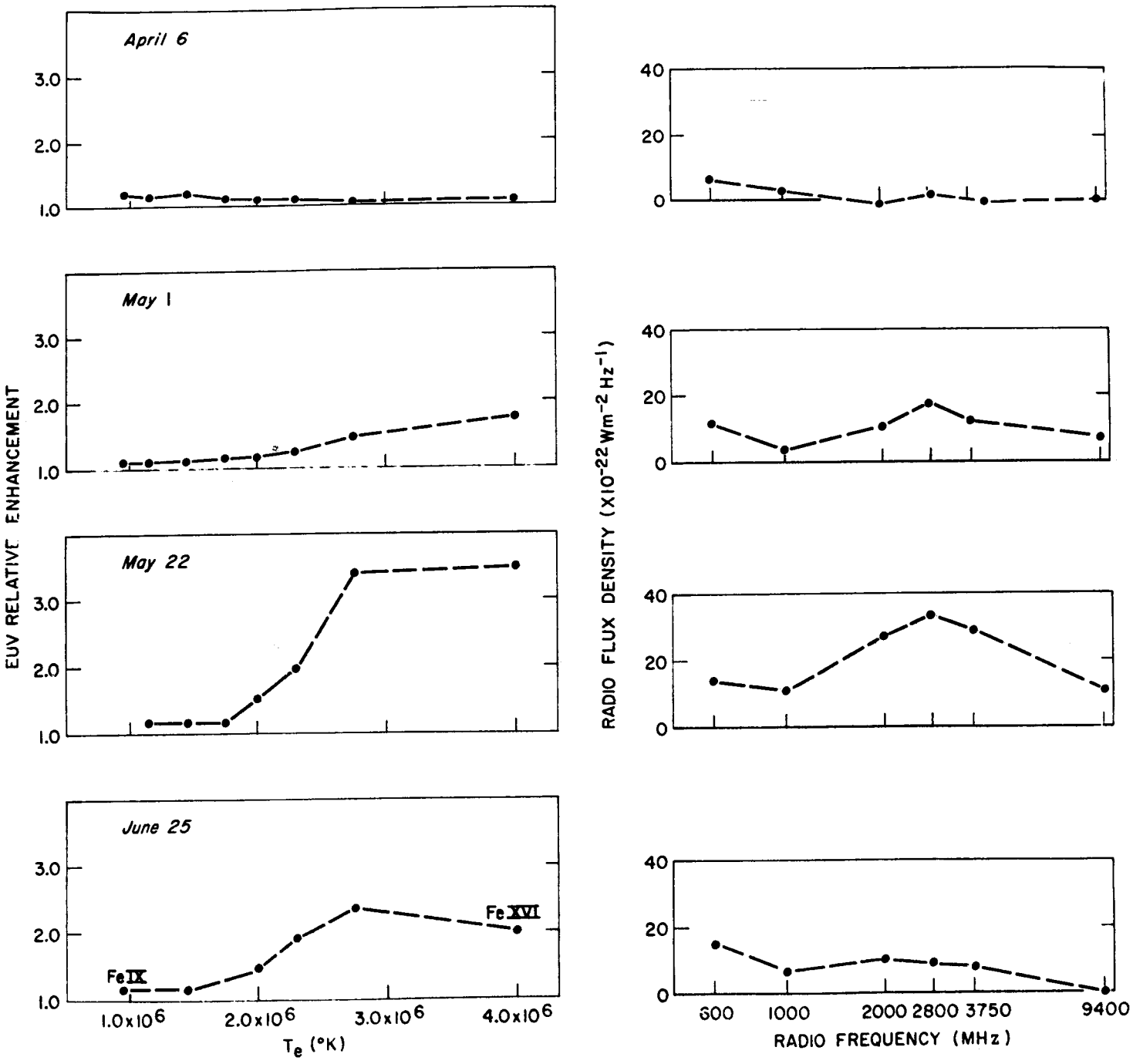
April 6
May 1
May 22
June 25
EUV RELATIVE ENHANCEMENT
3.0
2.0
1.0
Fe IX
Fe XVI
1.0x10^6
2.0x10^6
3.0x10^6
4.0x10^6
Te (°K)
RADIO FLUX DENSITY (X10^-22 Wm^-2 Hz^-1)
40
20
0
500
1000
2000
2800
3750
9400
RADIO FREQUENCY (MHz)

this region, but the last observations made in May, on May 22, only two days after reappearance of the active center on the east limb, are included in Figure 3 for completeness. A final observation, of lesser reliability, was made on June 25. Sunspot activity had ceased by this time and EUV and radio fluxes were diminishing.

A second sequence of observations, corresponding to central meridian passage of a different solar longitude is given in Figure 5. Sunspot and CaII plage characteristics of the three major active regions observed in this sequence are given in Table II. The development of these three regions was already underway when they were first observed by OSO-1 on the east limb on March 17. At central meridian passage, on March 24, only one region (Region II in Table II) containing the E spot group (large bipolar group having complicated structure, the two major spots each showing a penumbra) showed signs of flare activity. These regions were subsequently observed on two subsequent central meridian passages on April 20 and May 17. On April 20, only the leading region (Region I) in the northern hemisphere was a site of flare activity and was similar with respect to sunspots and CaII plage to region II on March 24. By May 17 all sunspots had disappeared and only CaII plage remained to mark the positions of the three regions. It appears that these three regions follow the typical pattern of rapid rise to a phase of maximum activity and sunspot complexity with a

TABLE II. MAJOR ACTIVE REGIONS OBSERVED BY OSO-1

	March 24	April 20	May 17
Region I			
McMath Region	6370	6393	6417
Position	N09 W14	N10 W22	N11 W23
Zurich Sunspot Class	C11	E38	None
Ca II Plage Area	2300 *	5600	3300
Region II			
McMath Region	6373	6395/6398	6419/6421
Position	N12 E10	N08 E03/N15 E20	N11 E05/N17 E25
Zurich Sunspot Class	E35	B5/B4	None/None
Ca II Plage Area	6000	3900/4100	2200/2600
Region III			
McMath Region	6369/6372	6394/6396/6397	6420/6422
Position	S13 E05/S02 E05	S10 W06/S11 E08/S12 E23	S10 E02/S12 E27
Zurich Sunspot	A8/None	A2/None/None	None/None
Ca II Plage Area	7000/1100	1200/800/800	1400/900

*Millionths of the Solar Disk

subsequent slower decline first described by Keipenheuer (1953). In spite of the mixture of different levels of activity in regions observed simultaneously, the microwave and EUV flux variations with time were similar to those of the first group of regions (Figure 4). The radio spectrum became flatter and the maximum EUV enhancement passed from Fe XVI to Fe XV as the group of regions declined in activity.

From the first group of data, given in Figure 4, the EUV and microwave fluxes associated with the active center observed on May 1 (C11 spot group) can be obtained directly. Subsequent development of this region was not reliably observed. A more complete analysis is possible using the second group of data (Figure 5). Starting with data taken on May 17, we assume that the increase in emission over that observed from the undisturbed corona (March 9-11) can be associated primarily with three old "quiescent", regions which are no longer the sites of flare activity and sunspots. The flux attributable to each of these regions can be taken to be one-third of the total relative enhancement observed on May 17. Upon going back one solar rotation we observe that all three of the quiescent regions observed on 17 May are already in existence on April 20, at which time flare activity is associated with only one (Region I) of the three regions. The other two regions (Regions II and III) contain small spot groups (Zürich Type A) which, consistent with the description given by Kiepenheuer, are very slowly diminishing in number and in size. The ultraviolet emission from Region I can be obtained by subtracting from the total

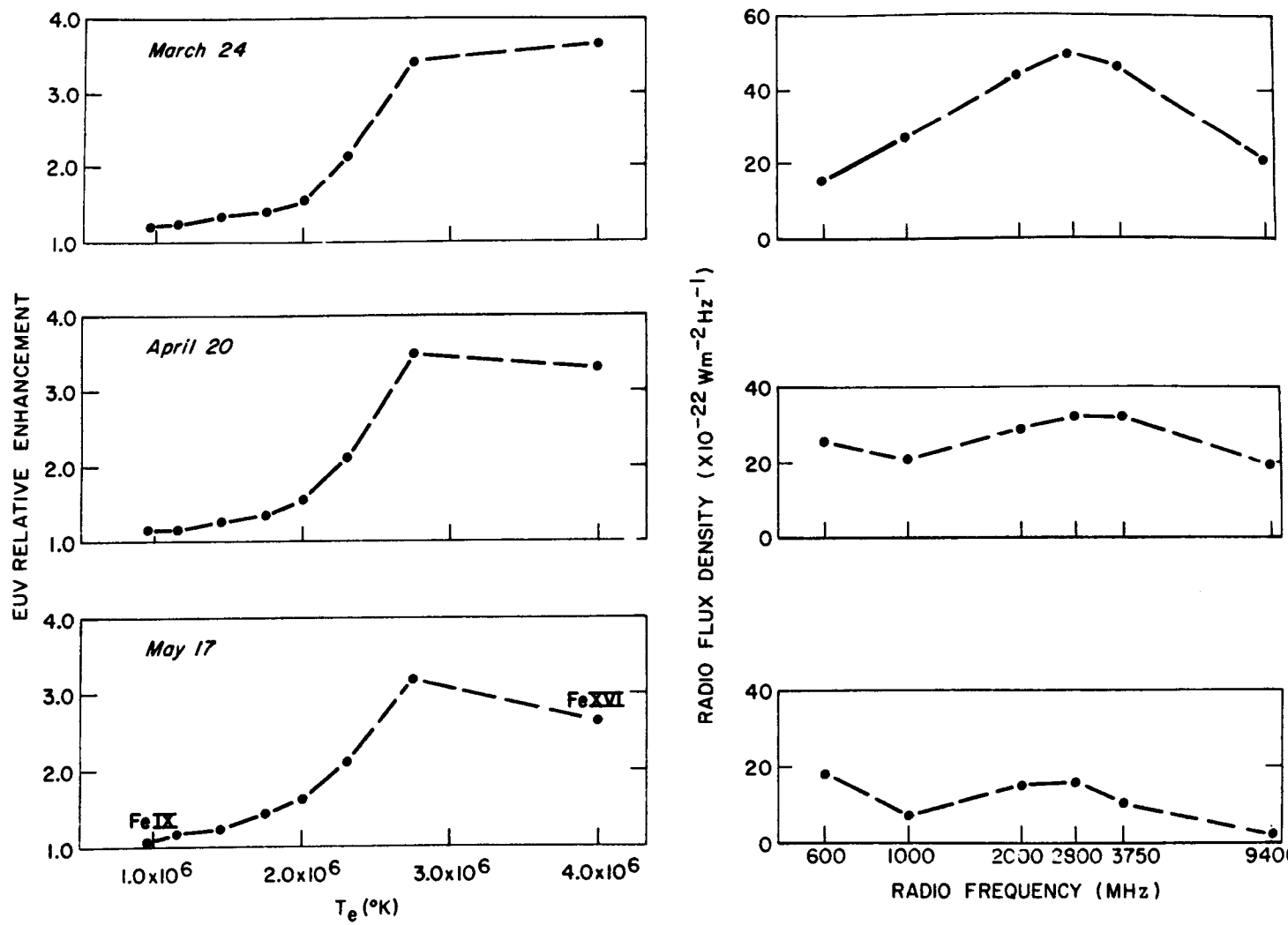
March 24
April 20
May 17
Fe IX
Fe XVI
EUV RELATIVE ENHANCEMENT
4.0
3.0
2.0
1.0
1.0x10^6
2.0x10^6
3.0x10^6
4.0x10^6
T_e (°K)
RADIO FLUX DENSITY (X10^-22 Wm^-2 Hz^-1)
60
40
20
0
600
1000
2000
2800
3750
9400
RADIO FREQUENCY (MHz)

increase observed on April 20 an estimate of the emission associated with Regions II and III. To obtain this estimate, we have assumed that (1) in the last phases of activity in a region the EUV and radio emissions change only slowly over a period of weeks and (2) for a given level of activity, the emission from the corona is directly proportional to the CaII plage area associated with the active region. Thus the fluxes from Regions II and III on April 20 are estimated using the observations made on these same regions one solar rotation later and this estimate is 50% greater than the value obtained on May 17, corresponding to the 50% greater CaII plage area reported for these regions in April. The data for March 24 can be treated in a similar manner, by subtracting from the total observed increase an estimate of the emission from the region over the E spot group located near the meridian on that date, using the result we have just obtained for a comparable region (Region I) in April. The residual flux is to be associated with two other large regions (C11 and A8 spot groups) observed near the meridian on March 24. After introducing an estimate for the probable emission from two small spot groups on the sun on May 17 which were not included in the analysis, we obtain the results given in Figure 6. The increases are again given in units of the flux from the sun as observed on March 9-11. It should be reiterated that we have used several similar solar regions in arriving at these results. The time scale used in Figure 6 therefore does not apply to any one particular region observed throughout its entire lifetime, although it is correct for the development of Region III (of Table II) which was observed in the southern hemisphere. The northern hemisphere active regions observed

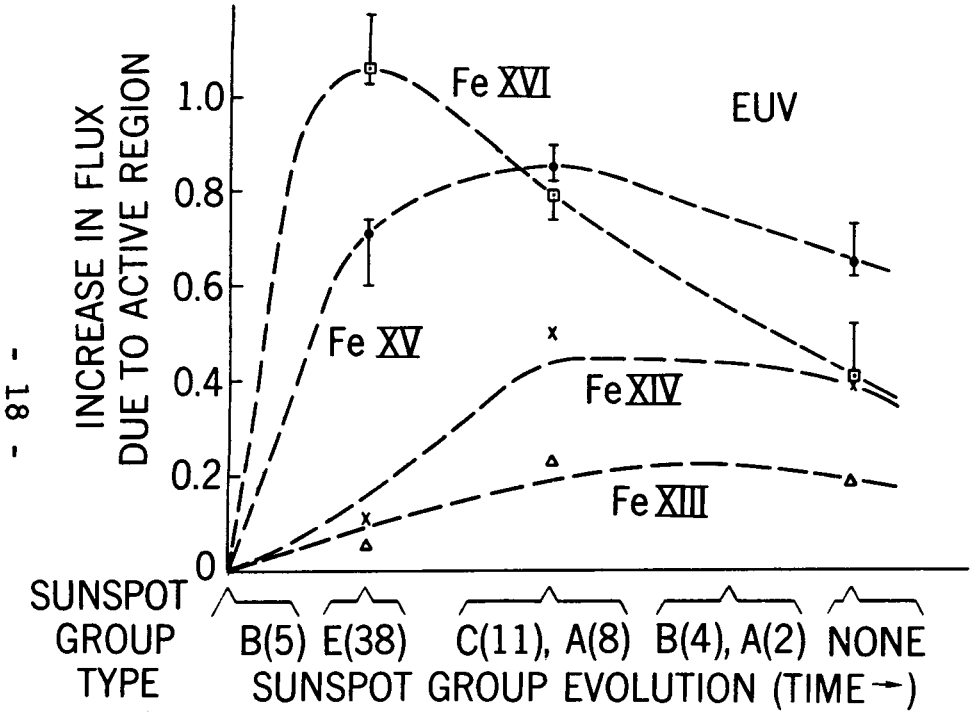
INCREASE IN FLUX
DUE TO ACTIVE REGION
1.0
0.8
0.6
0.4
0.2
0
Fe XVI
Fe XV
Fe XIV
Fe XIII
EUV
SUNSPOT
GROUP
TYPE
B(5) E(38) C(11), A(8) B(4), A(2) NONE
SUNSPOT GROUP EVOLUTION (TIME→)

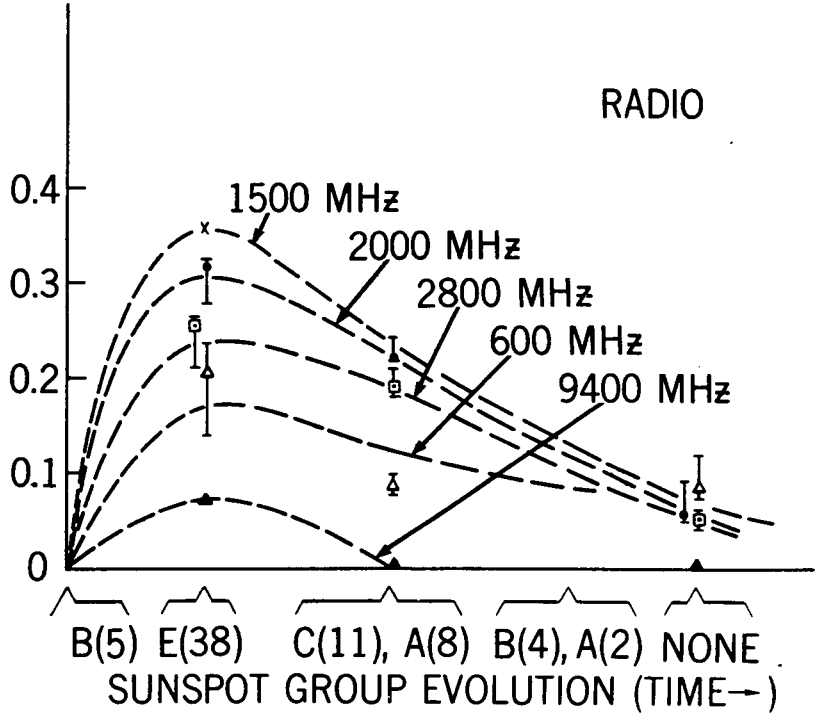
RADIO
0.4
0.3
0.2
0.1
0
1500 MHz
2000 MHz
2800 MHz
600 MHz
9400 MHz
B(5) E(38) C(11), A(8) B(4), A(2) NONE
SUNSPOT GROUP EVOLUTION (TIME→)

on March 24 and April 20 are recurrent in that they occur in the same location (or nearly so) as several previous active centers. Since the periods of activity are separated in time by a well defined interval during which no flares occurred in the region, we feel justified in defining the age of these two active centers as measured from the beginning of renewed activity. In all cases we present the sunspot information associated with each EUV enhancement.

The time dependence of the radio emission, as shown in Figure 6 generally confirms earlier observations made by Vauquois (1959). The highest reported frequency (9400 MHz) is emitted almost exclusively during the period of highest activity, while the lowest frequency persists even after sunspots have disappeared. Only weak, or, in most cases, no polarization of the radio emission was observed during the interval of March - May 1962.

Of all the radiations investigated in this paper, it appears that the fluxes from Fe XVI and Fe XV show the greatest increases over active regions. More precisely, it appears that the greatest increase is associated with the highest stage of ionization, at the time of maximum development of the sunspot group. The similarity of the Fe XVI and decimetric radio results extends also to solar flares accompanied by ionospheric effects (Neupert, 1965). In that case the time of maximum emission and total duration of Fe XVI emission coincides with the "gradual rise and fall" observed at decimetric wavelengths. The emission

lines from Fe XIV and Fe XIII associated with a region are observed to reach a maximum after the peak of flare activity. Below Fe XIII, the ultraviolet increases are small and less well correlated with the appearance of active centers.

The time dependence uncovered for Fe XIV has prompted us to analyze limb observations of the λ5303 line of that ion. Isophotes of Fe XIV emission constructed from observations made at Climax, Sacramento Peak, Pic du Midi and Kiskolovodsk are presented in Figure 7 and support the conclusion that λ5303 was more intense in April and May than in March, and that the maximum intensities occurred after flare activity had subsided. We have no data for the coronal forbidden line of Fe XV at λ7059, while Fe XVI has no forbidden lines, so the EUV curves for these ions cannot receive direct support.

III. ANALYSES OF SOLAR OBSERVATIONS

A. EUV Line Emission

Assuming that an emission line is correctly identified, that the excitation rate is known, and that self-absorption in the line can be evaluated, the flux of radiation in that line can be used to estimate the number of ions in the upper level of the transition in that part of the sun's atmosphere visible from the earth. The flux of radiation, F, in the line is given by

$$F = \int L\ N_e N_Z dv / 4\pi A^2 \qquad (1)$$

1962 MARCH 24 | 1962 APRIL 20 | 1962 MAY 17

FRAUNHOFER INSTITUT MAPS

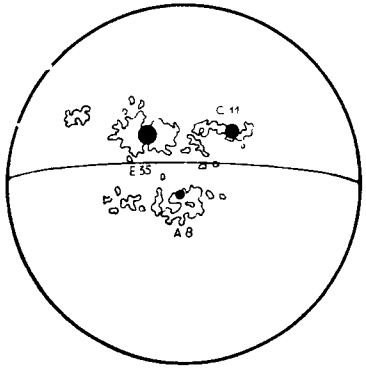

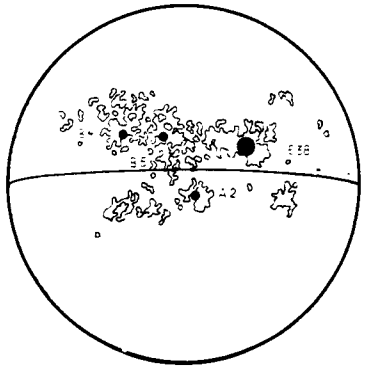

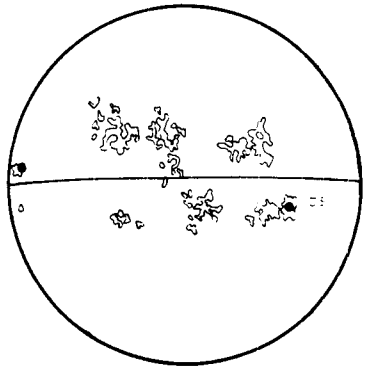

λ 5303 EMISSION

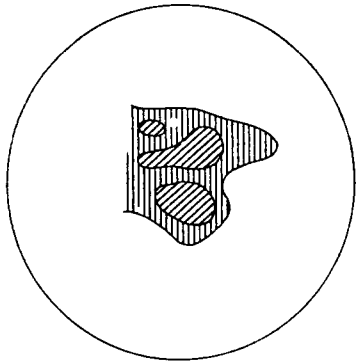

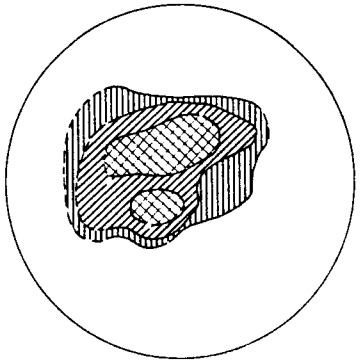

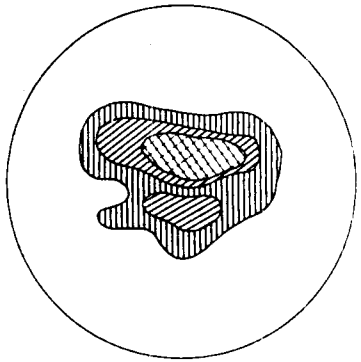

$I > 120 \times 10^{-6}$ OF THE SUN'S BRIGHTNESS

$86 \times 10^{-6} < I \leq 120 \times 10^{-6}$ OF THE SUN'S BRIGHTNESS

$55 \times 10^{-6} \leq I \leq 86 \times 10^{-6}$ OF THE SUN'S BRIGHTNESS

where L is the excitation rate per electron and ion, N_e is the electron density, N_Z is the ion density, A is the astronomical unit, and $\int dv$ is the integration over that part of the solar atmosphere visible from the earth. For the permitted transitions being discussed here, the population of the excited states is produced primarily by collisional excitation from the ground state. Using the collisional excitation rate given by Van Regemorter (1962) the flux at the earth is

$$F = 2.8 \times 10^{-43} f \int T^{-\frac{1}{2}} 10^{-5040\ W/T} N_Z N_e dv \qquad (2)$$

$$= 2.4 \times 10^{-43} f \int T^{-\frac{1}{2}} 10^{-5040\ W/T} \frac{N_E}{N_H} \frac{N_Z}{N_E} N_e{}^2 dv \qquad (3)$$

(Allen, 1965), where W is the excitation energy in ev and f is the oscillator strength of the line. N_E/N_H is the abundance of the element relative to hydrogen and N_Z/N_E is the fractional amount of the element in stage of ionization Z. The temperature terms can usually be removed from under the integral sign since the stage of ionization exists within a restricted temperature range. For a line which arises through collisional excitation from two levels of the ground term, such as λ270.5 of Fe XIV (the $3s^2\ 3p\ {}^2P_{\frac{1}{2}}$ - $3s\ 3p^2\ {}^2P_{\frac{1}{2}}$ transition), we use

$$F \propto \frac{f_{\ell 2 \leftarrow u}}{f_{\ell 2 \leftarrow 1} + f_{\ell 1 \leftarrow u}} \int (N_{\ell 1}\ f_{\ell 1 \rightarrow u} + N_{\ell 2}\ F_{\ell 2 \rightarrow u})\ N_e\ dv \qquad (4)$$

where $N_{\ell 1}$ is the population of the ground level of the lowest

term and $N_{\ell 2}$ is the population of the excited level of the same term (Stockhausen, 1965). The question of absorption of the radiation in the solar atmosphere has been considered by Ivanov-Kholodnyi and Nikolskii (1961) and Pottasch (1963). Each concluded that no correction for real absorption is necessary for the ultraviolet resonance lines. We will assume that the same holds true even for a localized emitting region of somewhat higher density.

We note that the measurement of a single ultraviolet emission line is insufficient to yield, simultaneously, information on the electron temperature, the elemental abundance, and the value of the integral $\int N_e^2\, dv$ for the region, or regions, in the corona from which the particular spectral line is emitted. If such coronal regions are essentially isothermal however, then the intensity ratio of two spectral lines emitted by adjacent stages of ionization can be used to obtain the relative populations in the ground states of these stages of ionization and hence an estimate of the coronal temperature, independent of elemental abundance and electron density, for the region emitting the lines. The pertinent processes of ionization and recombination which are balanced under steady state conditions have most recently discussed by Burgess and Seaton (1964), whose results for iron we use throughout this paper. Oscillator strengths for Fe XV and XVI have been derived from the absolute

multiplet strengths calculated for these transitions by Froese (1964), assuming, for Fe XVI, that the line strengths for the resonance doublet are in the ratio 2:1. Oscillator strengths for FeXIV have been calculated by Garstang (1962). The ratio $N_{\ell 2}/N_{\ell 1}$ has been found to have a value of approximately 0.15 (Jordan, 1966) and we have adopted this value.

B. Radio Emission

A study of solar decimetric and metric radio emissions provides sufficient additional information to construct a physical model of the corona above active regions. In contrast to the ultraviolet calculations, the absorption of radio emission in the solar atmosphere must be included in any calculation (Pawsey and Smerd, 1953). The apparent brightness temperature observed for any ray is given by

$$T_b = \int_o^\tau T_e(\tau) e^{-\tau} d\tau \qquad (5)$$

where the optical depth is

$$\tau = \int_S K(S) ds \qquad (6)$$

S being the path length along a ray and K(S) being the absorption coefficient. For sources in strong magnetic fields ($\gtrsim$ 500 gauss) both electron-ion collisions (Pawsey and Bracewell, 1955) and resonance absorption (Kakinuma and Swarup, 1962; Zheleznyakov, 1962) should be taken into account when calculating the optical depth. Assuming an isothermal corona

with an underlying isothermal chromosphere of infinite optical depth, the brightness temperature of a source at the center of the disk can be expressed by:

$$T_b = T_e\ (1-e^{-\tau c}) + Tch^{-\tau c} \qquad (7)$$

(Pawsey and Smerd, 1953) where τ_c, the optical depth of the corona can be calculated for various models from eq. 4 and T_e and T_{ch} are the electron temperatures of the (isothermal) corona and chromosphere, respectively. The average brightness temperature of a source can then be directly related to the observed flux density by:

$$I_\nu = 3.075 \times 10^{-28}\ \nu^2\ \Omega\ T_S \qquad (8)$$

(Unsöld, 1955) where Ω is the solid angle subtended by the source and T_S is its average brightness temperature.

The radio emission from an optically thin coronal source in a weak magnetic field is proportional to $\tau_c\ T_e$ and, because of the $T_e^{-3/2}$ dependence of the collisional absorption coefficient, may actually decrease slowly as the temperature is increased. For such a source, however, the emission varies with the square of the electron density. Under these circumstances the radio flux is sensitive to density changes of the emitting region. At decimetric wavelengths the emission originates in the lower portions of the corona over an active region and provides a means for estimating the average electron density in the volume which is emitting the EUV lines of Fe XV and Fe XVI.

We conclude then that the ultraviolet and radio observations complement each other: Whereas the radio data may give inconclusive results on the coronal electron temperature above an active region, the ultraviolet emission from several stages of ionization of an element is a sensitive indicator of temperature and temperature changes. On the other hand, the ultraviolet data cannot give information on electron densities unless the abundance of the emitting element is known, whereas the radio data do not have this drawback. The EUV data will yield information on elemental abundances once the densities and temperatures within the active region have been specified.

In using radio observations to estimate electron densities in the coronal regions emitting Fe XVI and Fe XV radiation, we assume that:

1) the radio frequency which yields the most accurate electron density information on the Fe XVI and Fe XV emitting regions is also the one whose flux variations with time correlate best with the variations in Fe XVI and Fe XV line emission as indicated in Figure 3. The frequency so chosen is 2000 MHz.

2) the lack of significant polarization of the radio emission implies that the emission is predominantly thermal, with electron-ion collisions being the primary absorption mechanism at 2000 MHz. The absorption coefficient used is that given by Pawsey and Bracewell (1955). At 2000 MHz the index of refraction for normal coronal densities is so

nearly unity that curvature of ray trajectories need not be considered.

3) the coronal region of enhanced electron density extends from 10,000 km. to 100,000 km above the photosphere. In this range of heights, the electron density is assumed to be that given by the Van de Hulst equatorial distribution, as modified by Newkirk (1961) for the last solar maximum, and multiplied by some factor, to be determined, which varies with the age of the active region but is independent of height.

4) the electron temperature of the chromosphere is taken to be 2×10^4 °K and that of the undisturbed corona to be 2×10^6 °K. The value of $\int N_e^2 dv$ deduced for the undisturbed corona from the radio data depends upon the specific temperatures which are assumed - a reduction by 25% in the chromospheric temperature requiring a 10% greater value of N_e throughout the corona to match the observed brightness temperature. On the other hand such a change in chromospheric temperature can be entirely offset by reducing the assumed coronal temperature to 1.2×10^6 °K. Obviously, such differences in the computed mean coronal density are of little significance in light of the known variations in electron density from equator to pole.

5) in obtaining the central brightness temperature, T_{bo}, of the quiet sun from the observed brightness temperature, T_{so}, of the quiet solar disk we apply the ratio of 0.665 (at 2000 MHz) determined by Piddington (1951) and also Allen (1957).

6) the model active region is assumed to cover an area which contains the bright Ca II plage associated with solar activity. For young regions, this area is equal to the plage area. Observations by Tousey (1965) that Fe XV and Fe XVI emissions are strongly localized over bright plages form the basis for assuming that the increased fluxes in these two stages of ionization as well as the radio emission at 2000 MHz originate in the same volume of the corona above active regions. For older regions, in which the Ca II plage appears as disconnected, fainter patches, the assumed area is taken to be that of one region which contains all plage associated with the active center. This assumption is consistent with the λ5303 limb observations of Fe XIV (see Figure 7) and the Fe XV and Fe XVI observations discussed earlier. In this manner it was determined that the coronal enhancement associated with the active region of April 20, 1962 covered 1.15% of the visible solar disk and each of the regions of 17 May 1962 covered 3.18% of the disk. The mean coronal density for the undisturbed sun was estimated by matching the observed central brightness temperature, T_{bo}, to a calculated temperature, based on equations 5-8 and the Newkirk electron density distribution, this distribution being scaled by some constant factor to produce a good agreement. The apparent brightness temperature of the disturbed sun was expressed as:

$$T_s = T_{so} - AT_{bo} + AT_a$$

where A is the area appropriate for the model active region and

T_a is its brightness temperature at central meridian passage. The electron density in the active region was obtained by determining the increase in density necessary to account for the increase in radio emission over that observed for the quiet corona.

IV. A MODEL OF THE SOLAR CORONA ABOVE ACTIVE REGIONS

The results from OSO-1 are most reliably applicable to estimate the mean temperature and density above a) an active E-spot region and b) an old plage (quiescent region). We obtain the electron temperature from the relative enhancements observed for λ335 (Fe XVI), λ284 (Fe XV), and λ270.5 (Fe XIV) given in Figure 6. We then use the radio emission to estimate electron densities both for the quiet corona and for the active region. The temperature and densities so obtained are combined to estimate the abundance of iron over active regions from the EUV emission. The conclusions will not be correct during the occurence of flares or other transient phenomence. Neither will they be correct for structures with high temperature gradients, such as loops or prominences above active regions. However the consistent use of intense emission lines and the most intense portion of the radio spectrum may insure that the following conclusions are valid for the bulk of the material in the corona above active regions.

The electron temperatures derived from the satellite observations are given in Table III. Temperatures deduced with and without the inclusion of the dielectronic recombination process

TABLE III. CORONAL ELECTRON TEMPERATURES ABOVE ACTIVE REGIONS

	Bright Ca II Plage (Type E Spot Group)	Weak Ca II Plage (No Sunspots)
WITH DIELECTRONIC RECOMBINATION (1)		
Fe XVI/Fe XV	3.8×10^6 °K	2.9×10^6 °K
Fe XV/Fe XIV	4.0×10^6 °K	2.5×10^6 °K
WITHOUT DIELECTRONIC RECOMBINATION (2)		
Fe XVI/Fe XV	1.6×10^6 °K	1.3×10^6 °K
Fe XV/Fe XIV	1.7×10^6 °K	1.3×10^6 °K

(1) Burgess and Seaton (1964)

(2) House (1964)

are given. We conclude that the coronal temperature reaches a maximum at the time of greatest spot complexity and coincident with the time at which flare activity is most likely to occur (observations which showed an increase directly attributable to a specific flare event were extremely few in number, about 1%, the total number of observations used.)

An unexpected result is that the electron temperature deduced using Fe XIV and Fe XV is the same as when Fe XV and Fe XVI are used. One might expect that the lower the stage of ionization the lower the electron temperature which will be deduced. Our only explanation is that the increase in electron density over the active region may be sufficiently large to more than compensate for a decrease in population of a stage of ionization produced by an increase in temperature. Under these circumstances an increase in Fe XIV radiation will be observed even if the temperature is greater than that required to maximize the population in this stage of ionization. This conclusion is consistent with observations of enhanced Fe XIV λ5303 emission, with broadened profiles, however, in regions where the Ca XV yellow line (λ5694) is also observed. (Billings, 1966) The estimate of 3.5 - 4.0 x 10^6 $^\circ$K above an E spot group observed on 24 March is comparable to the value of 3.5 x 10^6 $^\circ$K inferred from the Doppler broadened visible line of Ca XV (Billings, private communication), obtained when the E Spot group of March 24 had moved to the western solar limb on March 31. Of course, the comparison loses much of its meaning because of the non-simultaneity of the two measurements,

and the possibility that the Ca XV emitting region may be at a higher temperature than that from which the Fe XVI originates.

The EUV derived electron temperatures are higher, by a factor of two, than the observed radio brightness temperature at 2000 MHz. The value of 1.9×10^6 °K, corresponding to an optical depth of 0.6 at 2000 MHz, deduced for the April 20 region is however altogether consistent with the range of radio brightness temperatures (1.6 to 3.8×10^6 °K) inferred for such regions at a slightly higher frequency, 2800 MHz, by Swarup et al. (1963). Previous efforts to deduce electron temperatures in the corona above active regions from radio observations had led to results which were at variance with one another as well as with temperatures deduced optically by ascribing the observed spectral line profile to Doppler broadening. Calculations made by Waldmeier and Müller (1950), and Newkirk (1961) assumed electron densities estimated from optical observations, the former using eclipse observations and the latter K-coronameter data. Radio emission from the resultant models were then calculated for a range of electron temperatures. Waldmeier and Müller found that a temperature of 6×10^6 °K gave the best results while Newkirk found a temperature of $1\text{-}2 \times 10^6$ °K to be satisfactory. Christiansen et al (1960) used the observed ratio brightness temperature size, and height of emitting regions over a range of frequencies to build up the density and temperature distribution in the range from 10,000 km to 300,000 km, above the photosphere. These authors found a temperature of 1.5×10^6 °K at 300,000 km rising to 2×10^6 °K at 15,000 km, then falling rapidly to chromospheric values.

Piddington and Minnett (1951) on the other hand, considered the effect of a magnetic field in increasing the height of the emitting region at a given frequency and found that a temperature of 10^6 °K gave generally satisfactory results between theoretical and observed values of the radio emission. Setting aside for the moment the possibility that these authors were observing atypical active regions, thus arriving at rather disparate results for the electron temperature, we note that the radio emission from optically thin sources is dependent on temperature only as $T^{-1/2}$ and is therefore an insensitive means for determing this parameter. The data obtained in this paper suggest that the corona above active regions is not always optically thick at 2000 MHz, but when it is, the limiting radio brightness temperature should agree well with the electron temperature deduced from EUV line intensities.

As activity diminishes, the electron temperature decreases slowly. For the regions observed by OSO-1, the period of maximum activity is of the order of two weeks long whereas the following interval of diminished activity is two months or longer. The electron temperature of 2.5 - 3.0 x 10^6 °K deduced for the latter interval is still significantly above the range of temperatures usually associated with the undisturbed corona.

Of interest in this regard are the Fe ion distributions calculated by Burgess and Seaton. At 3.8 x 10^6 °K they find iron to be distributed at 4% Fe XIV, 15% Fe XV, 40% Fe XVI and about 35% (estimated by us) Fe XVII . At the lower temperature of 2.8 x 10^6 °K, they find 17% Fe XIV, 28% Fe XV (maximum for this

ion) 28% Fe XVI and about 18% (estimated) Fe XVII. The temperature for maximum Fe XIV abundance is 2.3×10^6 °K. By way of comparison, Billings (1959) finds that the most prevalent λ5303 profile, interpreted as Doppler broadening, corresponds to a temperature of 2.4×10^6 °K.

Finally, with diminishing activity the radio brightness temperature decreases markedly (See Table IV). This is the result of the reduced optical thickness (0.06 at 2000 MHz for the corona above quiescent regions) which, as we have pointed out, is most strongly dependent on electron density rather than electron temperature. We have observed no rapid decreases in electron temperature having a time scale comparable to the theoretical relaxation time of the corona (of the order of a few days). This suggests that the slow decrease may actually represent a slow reduction in the rate at which energy is transferred into the corona above the active region.

ELECTRON DENSITIES IN THE CORONA ABOVE ACTIVE REGIONS

The radio measurements yield an estimate of the average electron density of the quiet corona, about 2/3 that observed for the solar equator at sunspot maximum (Newkirk, 1961), which is in keeping with our knowledge of coronal density variation between sunspot maximum and minimum (Van de Hulst, 1953). This estimate forms a basis, although one of limited physical significance, to which we can compare densities observed above

TABLE IV. PROPERTIES OF CORONAL MODELS

	ACTIVE REGION	QUIESCENT REGION	UNDISTURBED CORONA
Associated Sunspot Group	E38	NONE	NONE
Diameter of Active Region	150,000 Km.	250,000 Km.	
T_e (EUV Data) (1)	$3.8 - 4.0 \times 10^6$ °K	$2.5 - 2.9 \times 10^6$ °K	$\approx 1.0 - 2.0 \times 10^6$ °K
T_b (2000 MHz Radio Data)	1.9×10^6 °K	1.8×10^5 °K	4.4×10^4 °K
Mean Electron Density	$11.2 - 12.2\ n_q$	$2.8 - 3.4\ n_q$	$n_q \approx 0.66$ of Newkirk's n_e at sunspot maximum

(1) Burgess and Seaton (1964)

active regions. The estimated electron density of 9×10^9 cm^{-3} at a height of 20,000 km above an E spot group is consistent with typical results obtained by optical observation of such regions on the solar limb. In our case the region was observed by Billings on the western solar limb on 1 April. At limb passage a very active H-alpha loop, and also yellow line emission was observed. Billings (1963) estimated the electron density to be about 2×10^{10} cm^{-3} in a region extending 50,000 km along the limb (approximately one-half the meridional extent of the underlying plage at central meridian passage) and at a height greater than 20,000 km. Assuming this density is maintained over a height of 10,000 km, this observation yields

$$\int N_e^2 dh = 4 \times 10^{29} \text{ cm}^{-5}$$

over the Ca II plage. The increased densities in our model correspond to a value of

$$\int N_e^2 dh = 1.3 \times 10^{29} \text{ cm}^{-5}$$

This is to be compared with values of the integral of 1.3×10^{29} for a plage of intensity 3 (McMath-Hulbert scale) and 1.6×10^{29} for a plage of intensity 3.5 which were deduced by Kawakata (1960) from radio emission for sources observed during the last sunspot maximum (1957-1959). On the other hand, the Waldmeier and Müller (1950) original model for a coronal condensation yields (for an upright cylinder having the same $\int N_e^2 dV$ as their spherically symmetric model) a value of 3.0×10^{28} cm^{-5}. More

recently, Waldmeier (1962) has discussed in detail the coronal condensation observed at the total solar eclipse of February 5 1962. The electron densities he has inferred from the scattered photospheric radiation at the center of the condensation are comparable to the average densities in this paper.

With cessation of activity the coronal region becomes less dense. The residual Ca II plage is the last visual indication of slightly increased densities (a factor of 2 to 3) and an electron temperature of about 2.5 - 3 million degrees. Ivanov-Kholodnyi and Nikolskii (1963) have concluded that in the coronal regions above plage, which they label without further discrimination as active regions, the density is higher for a given value of T_e than in unperturbed regions. This is certainly true for both the active and quiescent region models we have developed. On the other hand, we cannot support for their further conclusion, arrived at by extrapolation of the brightness gradient of the H_{27} line at λ3666 given by Thomas and Athay (1961), that the temperature gradient of the lower corona above active regions is less than that of the undisturbed corona. The basic disagreement lies in the assumption made by Ivanov-Kholodnyi and Nikol'ski that the contrast between active and undisturbed corona was the same for all coronal emission lines. This led them to the conclusion that, for any electron temperature, the density of the active corona is increased by a constant factor over that of the undisturbed corona. In point of fact, however, the

OSO-1 data (Figure 2) demonstrate dramatically that some stages of ionization of an element increase much more than others, and we have shown in the present paper, that these increases appear to depend on the particular level of activity which exists. The EUV data suggest that above active regions a relatively smaller fraction of the value of the integral $\int N_e^2 dV$ comes from temperature between one and two million degrees; i.e., that the temperature gradient between chromosphere and the corona must be greater for the active region that for the undisturbed corona.

One may question whether the foregoing analysis, based on 3 days of observation out of the total of 65 days when the satellite was in sunlight and spacecraft tape recorders were functioning, represents typical conditions of the corona above active centers. To answer this, we have used the results of Figure 6 to predict the solar EUV flux in the λ335 and λ284 lines on days which were not used in the original analysis. The assumed sizes and heights of the emitting regions were strictly consistent with our previous assumptions except that for regions further than 65° from the central meridian we used the Ca II plage area as observed at 65° or less. For regions behind the solar limb we assumed that the entire region was localized at the position of the center of the region and estimated the radiation observable using the distribution of electron density with height which we have used in the foregoing analysis. The estimates of Fe XVI counting rates and the ratio of Fe XVI and Fe XV counting rates are compared to actually observed values in Figure 8. The generally satisfactory agreement over

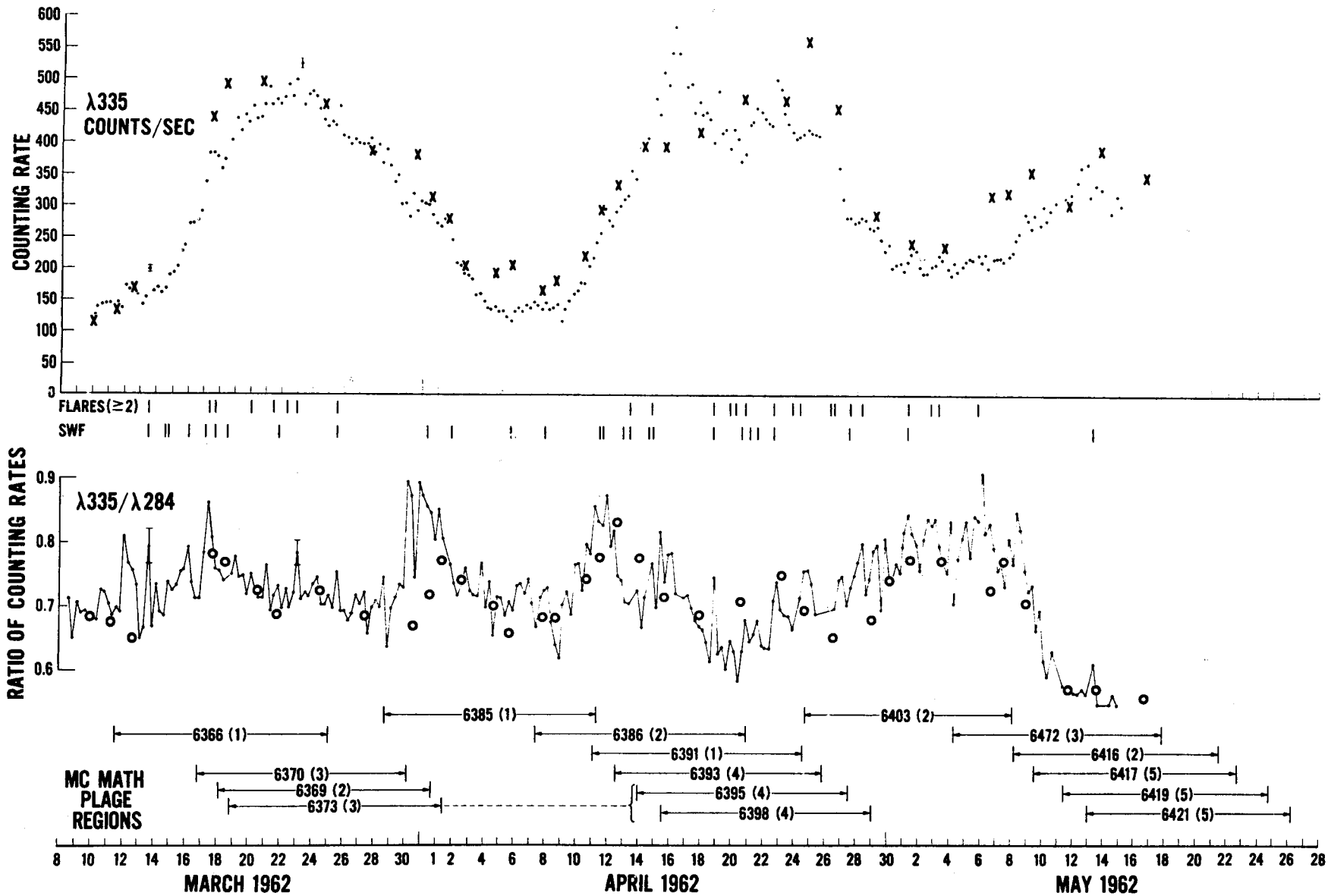
λ335
COUNTS/SEC
COUNTING RATE
600
550
500
450
400
350
300
250
200
150
100
50
0
FLARES(≥2)
SWF
λ335/λ284
RATIO OF COUNTING RATES
0.9
0.8
0.7
0.6
MC MATH
PLAGE
REGIONS
6366 (1)
6370 (3)
6369 (2)
6373 (3)
6385 (1)
6386 (2)
6391 (1)
6393 (4)
6395 (4)
6398 (4)
6403 (2)
6472 (3)
6416 (2)
6417 (5)
6419 (5)
6421 (5)
8 10 12 14 16 18 20 22 24 26 28 30 1 2 4 6 8 10 12 14 16 18 20 22 24 26 28 30 2 4 6 8 10 12 14 16 18 20 22 24 26 28
MARCH 1962
APRIL 1962
MAY 1962

the entire period of observations leads us to believe that the data we have used in our analysis represent typical coronal emission and that the solar variation of coronal emission with time, as implied by Figure 6, is verified by the bulk of these data.

ABUNDANCE OF IRON

Having obtained estimates of the average electron temperature and density increase in the corona above active regions, we are in a position to estimate the abundance of iron from the intensity of the EUV resonance lines. For the model active region, we obtain $\log N_{Fe}/N_H = 7.2 \pm 0.3$ and for the quiescent region, $\log N_{Fe}/N_H = 7.5 \pm 0.3$. The error stated here is the maximum uncertainty introduced by the method used to obtain the EUV fluxes from the coronal regions, i.e. the uncertainties indicated in Figure 6. An additional uncertainty, which we estimate as 50% is associated with the absolute calibration of the spectrometer for the λ284 and λ335 lines. This uncertainty does not exist for a comparison of the above iron abundance with the value of 7.60 obtained by Pottasch since the spectrometer used in the current study was "calibrated" by comparing its output with that of a calibrated rocket instrument flown by Hall et. al (1964) under similar solar conditions. The use of short wavelength ultraviolet lines for determining abundances should perhaps be questioned until further confirmation measurements of the absolute line intensities become available.

V. CONCLUSION

Extreme ultraviolet observations from above the atmosphere have provided a means for observing coronal regions of increased temperature and density as these regions pass across the solar disk. In this paper the observations of OSO-1 are used in conjunction with radio data to provide estimates of coronal density and temperature associated with several levels of solar activity. The current analysis is limited by the lack of spatial resolution and the uncertainties in calibration of the instrument. Improved instruments now being proposed and constructed should alleviate these problems.

I wish to express my gratitude for the support and encouragement given me by the late Dr. John C. Lindsay, Principal Investigator for the EUV spectrometer experiment on OSO-1 and Project Scientist for the OSO series of satellites. The development of the spectrometer was principally the work of my co-investigator, Dr. William E. Behring, supported by Mr. William A. Nichols, Mr. William A. White and other personnel of the Solar Physics Branch, Goddard Space Flight Center. Prof. Elske v. P. Smith, consultant to the Branch, has provided many stimulating discussions. I wish also to thank Mrs. Joanne Stanfill, Miss Diana Moseson, Mr. Charles Condor, and Mr. Michael Hantman for their painstaking work in analysing the nearly six thousand solar spectra on which this paper is based. The daily observations of solar activity made and reported by the McMath-Hulbert Observatory, The Fraunhofer Institut, and the many radio observatories are gratefully acknowledged.

REFERENCES

Alexander, E., Feldman, U., Fraenkel, B. S., and Hoory, S. 1965, Nature, 206, 176.

Allen, C. W. 1957, Radio Astronomy, I.A.U. Symp. No. 4, (Cambridge: Cambridge University Press), 253.

Allen, C. W. 1965, Sp. Sci. Rev., IV, 91.

Athay, R. G. 1966, Ap. J., 145, 784.

Austin, W. E., Purcell, J. D., Tousey, R., and Widing, K. G. 1966, Ap. J., 145, 373.

Behring, W. E., Neupert, W. M., and Nichols, W. A. 1962, J. Opt. Soc. Am., S2 (5): 597.

Behring, W. E., Neupert, W. M., and Lindsay, J.C. 1963, Space Research III ed. W. Priester, (Amsterdam: North-Holland Publishing Co.) p. 814.

Billings, D. E. 1959, Ap. J., 130, 961.

Billings, E. E. 1963, Private Communication.

Burgess, A., and Seaton, M. J. 1964, N. N., 127, 355.

Christiansen, W. N., Mathewson, D. S., Pawsey, J. L., Smerd, S. F., Boischot, A., Denisse, J. C., Simon, P., Kakinuma, T., Dodson-Prince, H. and Firor, J. 1960, An d'Ap., 23, 75.

Cowan, R. D., and Peacock, N. J. 1965, Ap. J., 142, 390.

Detwiler, C. R., Garrett, D. L., Purcell, J. D., and Tousey, R. 1961, Ann. Geophys., 17, 9.

Elton, R. C., Kolb, A. C., Austin, W. E., Tousey, R. and Widing, K. G. 1964, Ap. J. 140, 390.

Fawcett, B. C. and Gabriel, A. H. 1965, Ap. J., 141, 343.

Fawcett, B. C., Gabriel, A. H., and Saunders, P. A. H. Submitted for publication in Proceedings of the Physical Society.

Froese, C. 1964, Ap. J., 140, 361.

REFERENCES (Continued)

Gerstenberg, R. H. 1962, Ann. d'Ap., 25, 109.

Hall, L. A., Damon, K. R., and Hinteregger, H. E. 1963, Space Research III, ed. W. Priester, (Amsterdam: North-Holland Publ. Co.), 745.

Hinteregger, H. E. 1961, J. Geophys. Res., 66, 2367.

House, L. L. 1964, Ap. J., Suppl., Vol. VIII, 307.

House, L. L., Deutschman, W. A.and Sawyer, G. A. 1964, Ap. J., 140, 814.

Ivanov-Kholodnyi, G. S., and Nikol'skii, G. M. 1962, Soc. Astron., 5, 31, 632.

Ivanov-Kholodnyi, G. S. and Nikol'skii, G. M. 1963, Sov. Astron., 6, 609.

Jordan, C. 1966, Mon. Not. R. Astr. Soc., 132, 515.

Kakinuma, T., and Swarup, G. 1962, Ap. J., 136, 975.

Kiepenheuer, K. O. 1953, The Sun, ed. G. Kniper, (Chicago: University of Chicago Press), 322.

Kawabata, K. 1960, Publ. Ast. Soc. of Japan, 12, 513.

Kundu, M. R. 1959, Ann d'Astrophys., 22, 1.

Neupert, W. M., and Smith, E. v.P. 1964, Astron. J., 69, 554.

Neupert, W. M. 1965, Ann, d'Ap., 28, 446.

Newkirk, G. 1961, Ap. J., 133, 983.

Pawsey, J. L., and Smerd, S. F. 1953, The Sun, ed. G. Kuiper, (Chicago: University of Chicago Press) 466.

Pawsey, J. L., and Bracewell, R. N. 1955, Radio Astronomy (Oxford: Oxford University Press), 83.

Piddington, J. H., and Minnett, H. C. 1951, Aust. J. Sci. Res., A4, 131.

REFERENCES (Continued)

Piddington, J. H. 1951, M. N., 111, 45.

Pottasch, S. R. 1963, Ap. J., 137, 945.

Pottasch, S. R. 1966, Bull. Ast. Inst. Neth., 18, 237.

Stockhausen, R. E. 1965, Ap. J., 141, 277.

Swarup, G., Kakinuma, T., Covington, A. E., Harvey, G. A., Mullaly, R. F. and Rome, J. 1963, Ap. J., 137, 1251.

Thomas, R., and Athay, G., 1961, Physics of the Solar Chromosphere (New York: Interscience Publishers, Inc.) 392.

Tousey, R. 1965, Ann. d'Ap., 28, 755.

Unsöld, A. 1955, Physik der Sternatmosphären, 2 Aufl., (Berlin: Springer-Verlag).

Van de Hulst, H. C. 1953, The Sun, ed. G. Kuiper, (Chicago: University of Chicago Press), 207.

Van Regemorter, H. Ap. J., 136, 906.

Vauquois, B. 1959, Paris Symposium on Radio Astronomy ed. R. N. Bracewell (Stanford, Calif., Stanford University Press) 143.

Waldmeier, M. 1947, Pub. Zürich Observatory, 9, 1.

Waldmeier, M., and Müller, H. 1950, Zeit. fur Astrophysik, 27, 58.

Waldmeier, M. 1962, Zeit. fur Astrophysik, 56, 291.

Widing, K. G. 1966, Ap. J., 145, 380.

Zheleznyakov, V. V. 1962, Sov. Astron., 6, 3.

Zirin, H., and Dietz, R. D. 1963, Ap. J., 138, 664.

FIGURE CAPTIONS

Figure 1. Two spectra obtained with the EUV Spectrometer on OSO-1. The emission lines indicated by wavelengths are prominent lines of highly ionized iron discussed in the present paper. Differences in the two spectra are attributable to active regions existing on the visible disk on March 22.

Figure 2. A comparison of solar EUV and radio emission in March-May 1962. The EUV data are normalized to observations made on March 9-11. The radio emission at each frequency has been reduced by the flux observed on these same days. The residual variations for both sets of observations correspond to the appearance of active regions as the result of solar rotation.

Figure 3. Results of a least squares fit of the EUV line emission to a quadratic function of the solar radio emission. The standard deviation of residuals obtained on the basis of a quadratic function is only slightly less than for a linear relation.

Figure 4. A sequence of iron emission line and radio observations made at monthly intervals during the development of active regions on the sun's visible disk. The sequence starts with the birth of a sunspot group on April 6. The EUV increases for each ion are plotted against the temperature at which that ion is most abundant in order to demonstrate the association between solar activity and coronal regions of increased electron temperature.

Figure 5. Sequential EUV and radio observations of another group of active regions. The birth of these regions occurred before the launch of OSO-I. The same normalization is used as in Figure 4. The Fraunhofer maps corresponding to these observations are given in Figure 7.

Figure 6. The EUV and radio fluxes attributed to an active solar region at various stages in its development. The increases in emission are expressed in terms of the total solar emission observed on March 9-11 in the absence of appreciable solar activity (Table I). Note that maximum emission in the highest observed stage of ionization coincides with maximum complexity

and size of the sunspot group. The time scale shown is typical for the type of region being discussed. Other such regions may have different rates of development.

Figure 7. Isophotes of λ5303 line emission (Fe XIV) for the dates used in the EUV analysis as constructed from limb observations. Associated Ca II plage regions and sunspot groups are shown on maps supplied by the Fraunhofer Institut for these dates.

Figure 8. Comparison of observed Fe XVI and Fe XV emission with predicted values (large symbols) based on models developed in the present paper. The ratio Fe XVI/Fe XV is used to suppress changes in coronal emission due to electron density changes and emphasize those associated with electron temperature changes. Sharp increases in this ratio, as on March 13, often coincide with solar flare associated "gradual rise and fall" observed at microwave frequencies.